Drag Analysis from PIV Data in Speed Sports

Terra, W.; Sciacchitano, A.; Scarano, F.

DOI
10.1016/j.proeng.2016.06.188

Publication date
2016

Document Version
Final published version

Published in
Procedia Engineering

Available online at www.sciencedirect.com

ScienceDirect

Procedia Engineering 147 (2016) 50 – 55

Procedia Engineering

www.elsevier.com/locate/procedia

11th conference of the International Sports Engineering Association, ISEA 2016

Drag analysis from PIV data in speed sports

W. Terra[a]*, A. Sciacchitano[a], F. Scarano[a]

[a]*Aerospace Engineering Department, Delft University of Technology, Kluyverweg 2, Delft, 2629 HT, The Netherlands*

Abstract

Aerodynamic drag is computed from velocity measurements obtained with particle image velocimetry (PIV). This allows determining the drag force in combination with the visualization of the flow structures responsible for drag generation. Two experiments are conducted to illustrate the working principle of the approach, which is meant for applications in speed sports. The first experiment assesses the aerodynamic effect of surface roughness by measuring the flow over a circular cylinder dressed in a rough fabric used in professional cycling. The application of roughness can reduce the drag by about 30% with respect to a smooth surface. The second experiment demonstrates at small scale a possible approach to directly study the aerodynamic drag associated to moving athletes. This offers an alternative to the measurements in wind tunnels, where only stationary cases are practically studied. A system towing a sphere of 16 cm diameter is used to demonstrate the concept. Drag coefficient calculations come to agree with literature data within 15%.

Peer-review under responsibility of the organizing committee of ISEA 2016

Keywords: aerodynamics; PIV; drag; speed sports

1. Introduction

Aerodynamics plays an important role in many speed sports, where races are won by fractions of seconds. In speed skating the aerodynamic drag can reach 80% [1] of the total resistance, in road cycling over 90% [2]. A small reduction of the aerodynamic drag can mark the difference between winning and losing a competition. For this reason the majority of the studies in speed sport aerodynamics deal with the quantification and minimization of aerodynamic drag [3].

The aerodynamic drag can be examined by wind tunnel measurements, field tests and numerical simulation (CFD). CFD has the advantage of providing whole-field data in addition to the aerodynamic forces. Whole-field information provides insight into the behaviour of the flow, from which a better understanding of the generation of the aerodynamic forces can be achieved [4]. Due to the complexity of the flow, however, the accuracy of numerical simulations is often questionable and model validation via experimental data is typically required. In field tests, the aerodynamic drag is estimated by measuring the generated mechanical power [5] or the oxygen intake [6] of the athlete. Accurate and repeatable drag measurements are mostly conducted in wind tunnels using force-balance systems. Despite their reliability, drag measurements alone using both field or wind tunnel tests do not give insight into the flow mechanism leading to the generation of drag.

Experimental investigation of the flow field is possible using particle image velocimetry (PIV). The air flow is seeded with microscopic droplets that are illuminated in short succession by two pulses of laser light. The light scattered by the particles is captured by a digital camera and computer analysis of the images yields the velocity field within a planar domain. Further analysis of the velocity field, in combination with the flow governing equations offers the possibility to extract the pressure in the flow or the overall aerodynamic force acting on the object [7]. PIV is nowadays used by thousands of research laboratories in various areas (e.g. aeronautics, biology, turbulence, combustion, wind

* Corresponding author. Tel.: +31-15-278-7095; fax: +31-15-278-7077.
E-mail address: w.terra@tudelft.nl

Peer-review under responsibility of the organizing committee of ISEA 2016
doi:10.1016/j.proeng.2016.06.188

energy), which has greatly stimulated its further developments [8]. Despite its success, PIV has to date found limited application in the field of speed sport aerodynamics. An example is due to Chabroux et al. [9] who used stereoscopic PIV to determine the wake characteristics of different time trial helmets used in cycling.

The present work discusses the use of PIV as a tool for the purpose of drag determination combined with the detailed visualization of the flow phenomena that play a role for the aerodynamic drag. This is relevant to the process of aerodynamic optimization. The discussion makes use of two experiments with different approaches to determine the drag from PIV data, which are envisaged for different sport applications.

The first application illustrates the reduction of aerodynamic drag by use of surface roughness of sport clothing. It is well known that the drag coefficient of bluff bodies varies with Reynolds number [10]. The drag coefficient envelope of smooth cylinders in cross flow exhibits a clear minimum around Re = 3.7 x 10^5, known as the drag crisis. Application of roughness on the surface of the cylinder anticipates the drag crisis to a lower value of the Reynolds number [11]. A shift of the drag crisis may decrease the drag of a cylinder over 50%. The flow around cylinders models that around certain body parts (e.g. arms and legs) of an athlete in motion. Oggiano et al. [12] showed that textiles with different roughness patterns are able to reduce the overall drag of the athletes. In this work, planar (two-dimensional) PIV measurements are conducted on a cylinder dressed with various fabrics used in professional cycling to quantify the drag reduction and illustrate the corresponding flow pattern.

The second application aims at demonstrating the feasibility to measure the flow field and associated drag directly around a moving athlete. In wind tunnel conditions, the most direct approach is that of measuring the drag force by a balance system connected to the model support [13]. In some cases wind tunnel measurements are unsuited, for instance due to the interference of model supports, the lack of a moving floor to represent ground velocity, the limited size of the accommodation, the accelerating motion of the athlete. Estimating the drag force by in-field measurements as described by Grappe et al [5] is a possible solution; however, separating the aerodynamic drag from the friction force between wheels and ground, requires assumptions that must be validated from case to case. A general drag measurement method for moving athletes does not exist to date, which is the overall aim of this study. The work presents the working concept that makes use of tomographic (three-dimensional) PIV measurements on moving athletes. The system is realized at reduced scale and the geometry considered herein is simplified to a sphere for the purpose of comparing the results with literature data.

2. Methodology

The time-averaged drag force acting on an arbitrary object in relative motion with respect to the surrounding fluid can be derived by the control volume approach [7, 14]. In fact, the mean drag can be derived solely from the velocity and pressure in a plane in the wake of the object, which extends sufficiently far into the outer flow:

$$\bar{D} = \underbrace{\iint_S (U_\infty - \bar{u})\bar{u}dS}_{\text{momentum term}} + \underbrace{\iint_S (p_\infty - \bar{p})dS}_{\text{pressure term}} \tag{1}$$

where the over-bar indicates the time average operation, D is the drag force, *u* the streamwise velocity and *p* the pressure. The first term on the right-hand side represents the momentum deficit occurring behind the moving object. The second term represents the pressure difference generated by the presence of the object that distorts the flow streamlines. The integrals are evaluated along the boundary of a domain enclosing the object. However, in practice, the integration can be reduced to the sole region downstream of the object if all the momentum deficit is captured and the surface is sufficiently far from the object.

Fig. 1 depicts schematically the situation. In front of the object the freestream conditions are defined by U_∞ and p_∞. Equation (1) holds for two- and three-dimensional stationary flows. According to the principle of Galilean invariance, it also applies to any frame of reference moving at constant velocity. Therefore this approach can be used to determine the time-averaged aerodynamic drag of an object moving at constant velocity [15].

The momentum term of equation (1) is directly measured with PIV. The pressure term, instead, needs to be reconstructed from the velocity data by solving the Poisson equation for pressure [7].

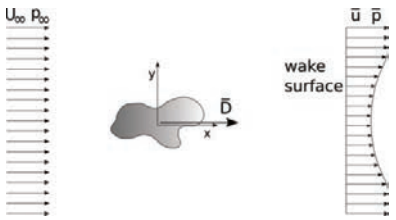

Fig. 1. Illustration of the control volume for momentum balance.

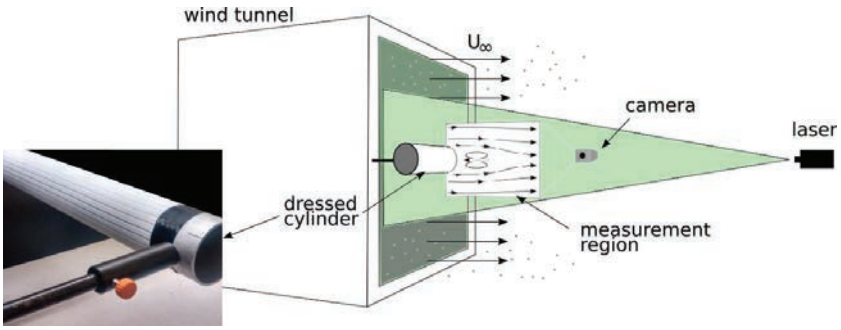

Fig. 2. Schematic experimental setup of planar PIV measurement around dressed cylinder with a photo of the dressed cylinder in the detail at the left.

3. Experiment 1: Drag reduction by application of surface roughness in sports clothing

3.1. Experimental setup and procedure

Planar PIV measurements are conducted on the flow in the wake of a cylinder in cross flow. The experiment is conducted in the W-tunnel of the Aerodynamics Laboratories of TU Delft. This low-speed, open-section wind tunnel has an exit cross section of 0.4 x 0.4 m^2 and turbulence intensity level of below 1%. Fig. 2 shows a schematic of the experimental setup. The cylinder is mounted at a distance of 20 cm behind the exit of the tunnel. The cylinder is 50 cm long and has a diameter of 7 cm. The flow over the cylinder is assumed to be two-dimensional considering its aspect ratio. In practise, some three-dimensional effects will be present and can affect the accuracy of the drag estimation. The free stream velocity is 25.5 m/s, corresponding to a Reynolds number of 1.19 x 10^5. This condition is selected such that the transition of the flow to the critical regime is only expected for the cylinder dressed in the rough fabric.

The flow is seeded with micron-sized droplets from a SAFEX smoke generator. Illumination is provided by a Quantel-Evergreen 200 laser. Hardware details and settings are listed in Table 1. The cylinder is dressed with two different covers, a smooth adhesive foil, and a fabric, used in time-trial suits in professional cycling, with a specific roughness pattern. A detail of the latter is shown at the left of Fig. 2. The fabric has wales of 6.6 mm width and 0.3 mm depth; the distance between the centre of two neighboring wales is 8.1 mm.

For both cylinder configurations, 200 images are acquired at an acquisition frequency of 2 Hz at two different camera positions; one camera contains the cylinder in its field of view, while the second camera position is further downstream. Velocity fields are reconstructed on interrogation windows of 16×16 pixels with 75% overlap using multi-pass cross correlation with Gaussian weighting.

Table 1. Hardware information and settings of the two experiments

	Experiment 1 - Planar PIV	Experiment 2 - Time resolved Tomo-PIV
Camera	PCO Sensicam 370LD double shutter (CCD)	4 Photron Fast CAM SA1 cameras (CMOS)
Resolution - pixel size [μm]	1280 x 1024 - 6.7	1024 x 1024 – 20
Recording rate [Hz]	2	250 Hz
lens	Tamron 35 mm	Nikkor 60 mm
f#	4	22
Laser	Quantel Evergreen 200 Nd:YAG (pulse energy 2x200mJ)	Quantronix Darwin Duo Nd:YLF (pulse energy 2x25 mJ at 1 KHz)
Field of view [mm^2 – mm^3]	350 x 260	200 x 300 x 160
Seeding	1 micron fog droplets	0.5 mm Helium-filled soap bubbles
PIV software	LaVision Davis 8	LaVision Davis 8
Velocity reconstruction	Multi-pass 2D cross correlation Interrogation windows of 16 x 16 pixels with 75% overlap	SMTE [18] tomographic algorithm with multi-pass 3D cross correlation Interrogation boxes of 64 voxels with 75% overlap
Number of samples used for time average	200	20

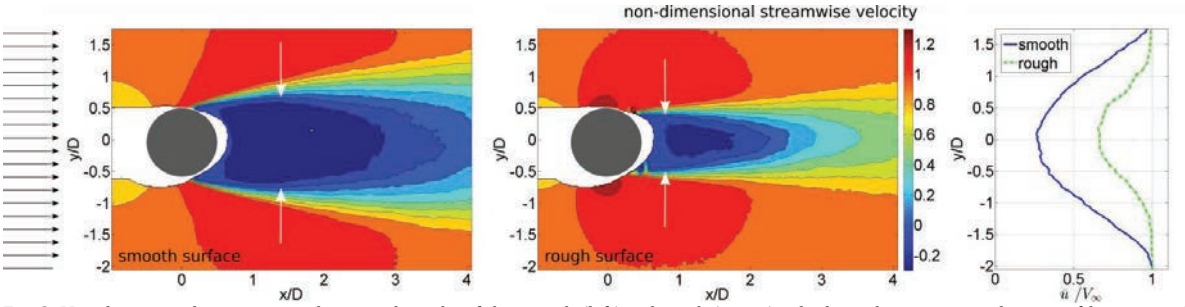

Fig. 3. Non-dimensional streamwise velocity in the wake of the smooth (left) and rough (centre) cylinder and streamwise velocity profiles extracted at x/D = 4 (right).

3.2. Results

The time average of the normalized streamwise velocity in the plane normal to the cylinder axis is shown in Fig. 3 for both cylinder configurations. Both velocity fields show a clear wake region, which is bounded by the contour of zero streamwise velocity. The maximum width of the wake is indicated with white arrows. The wake of the smooth cylinder is about twice as wide as that of the rough cylinder. Fig. 3-right presents profiles of streamwise velocity along the y-axis at a distance of four diameters behind the cylinder. Clearly the wake behind the rough cylinder is narrower and the momentum deficit is considerably lower, compared to the smooth cylinder, indicating a lower drag for the former. From this figure it is also observed that the flow in the wake of the smooth cylinder has not completely recovered to the freestream conditions at the edges of the measurement domain. This will influence the results of the drag and pressure computation, as recovery to the freestream is a needed condition within the present methodology to obtain an accurate estimate of the drag. The accuracy of the velocity reconstruction itself is quantified by reporting the mean, the standard deviation and the uncertainty of the mean of the streamwise velocity component outside the separated flow region at x/D = 0, y/D = 1.5; these are respectively $\mu = 1.02$, $\sigma = 0.07$ and $U_\mu = 0.006$ relative to the free-stream velocity.

The drag coefficient is computed with equation (1) at varying distance from the cylinder. The value of the drag should in principle remain constant and any variation will indicate the level of the uncertainty of its estimate. Furthermore the pressure term is expected to vanish at sufficiently large distance from the cylinder, while the momentum term shall reach an asymptotic value [14]. Fig. 4 presents the results of the computed drag coefficient for both cylinder configurations. The computed drag coefficient of the smooth cylinder varies with x/D (left figure). An asymptotic value is not reached for the momentum deficit, although the slope of this term appears to vanish when the value of this contribution tends to about 1.6. Contrary to what is expected, the pressure term does not vanish for increasing *x/D*, which is mainly ascribed to the limited size of the measurement domain: for large x/D, the flow at the edges of the domain does not recover to free-stream conditions, yielding significant errors in the drag estimated. Estimating the aerodynamic drag from a profile at *x/D* = 3.5, where free-stream conditions are approximately reached at the edges of the domain, yields a value of about $C_D = 1.1$. Previous works in literature report values of 0.9 [16], 1.1 [17] and 1.4 [11] depending on the specific model mounting, freestream turbulence and blockage. A relatively high freestream turbulence level and three-dimensional effects in the flow due to the open test section and the finite length of the model are sources of inaccuracies in our drag derivation.

From Fig. 4-right it is observed that the drag coefficient of the cylinder dressed in rough fabric reaches a relatively steady value of about 0.75 after x/D = 1.5, dominated by the momentum term. The pressure term rapidly decays after x/D = 1.5 and remains fluctuating around zero. The development of the individual terms matches the expectations much better. Compared to the smooth cylinder case, the drag is reduced by about 32%. Achenbach and Heinecke [11] report reductions of about 30% and Oggiano et al. [16] values between 22% and 36% for cylinders with varying roughness parameters.

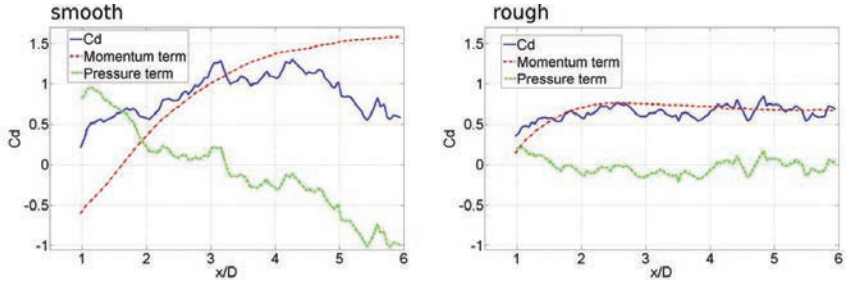

Fig. 4. Cylinder drag coefficient, momentum and pressure term computed at varying streamwise distances behind the cylinder for smooth (left) and rough surface (right).

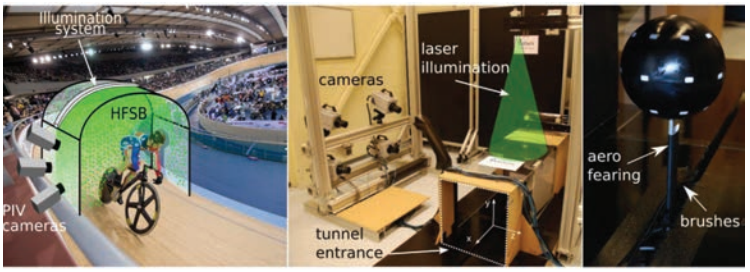

Fig. 5. Tomographic PIV measurement system; an illustration of the envisaged full-scale system (left); experimental setup (middle) and sphere model (right).

4. Experiment 2: Drag measurements on moving object

4.1. Experimental setup and procedures

A new concept for tomographic (three-dimensional) PIV measurements intended for the aerodynamic analysis and drag determination of moving athletes is depicted Fig. 5-left. Such a system is currently under development and the present work aims at illustrating its working principles. A proof-of-concept on a scaled version of the system is realized, which is schematically illustrated in Fig. 5-middle. The apparatus consists of a seeding particle container and a tomographic PIV system. The tunnel-shaped container is 170 cm long with a squared cross section of 50x50 cm^2. The container is partly made out of transparent Perspex to allow optical access for both illumination and imaging systems.

A sphere of 16 cm diameter (Fig. 5-right) is moved through the tunnel at a speed of about 1 m/s. The towing system is assembled using Lego® parts. A train transports the model along a rail through the container at constant velocity. The model is mounted on the train by an aluminum rod covered with an aerodynamic fairing to minimize flow separation and vortex shedding. The floor of the container contains a narrow opening in streamwise direction, which is covered by brushes. This zipper-like construction enables the sphere to transit through the tunnel and at the same time prevents an upward air flow into the container induced by the presence of the train.

Different time-resolved tomo-PIV measurements are conducted on the sphere passing through the tunnel. After each run the images that are taken in the wake of the sphere are used to reconstruct the instantaneous three-dimensional velocity field. The details of the PIV hardware, hardware settings and date processing are listed in Table 1. A Galilean transformation of the instantaneous velocity data is performed in order to reduce the data in a frame of reference consistent with the moving object. In this frame of reference, the time-averaged velocity field is obtained by averaging the data from twenty independent experiments.

4.1. Results

The time-averaged velocity computed from twenty uncorrelated data sets is presented in non-dimensional form in Fig. 6 showing contours of streamwise velocity in the central XY-plane (left) and a YZ cross-section selected at a distance of 1.25 diameters (middle) from the center of the sphere (located at x=0, y=0). From the figure on the left, a clear region of reverse flow is observed. The reattachment point is located at about x/D = 1.25, in fair agreement with values reported in literature; Jang and Lee [19] report a value of 1.0 and the work of Ozgoren et al. [20] shows a value of about 1.4. Accelerated flow is observed in the outer region around x/D = 0.5 and y/D = 0.8, which corresponds to the finding of Constantinescu and Squires [21]. Furthermore the wake is reasonably circular (Fig. 6-middle), indicating an acceptable level of statistical convergence for data time averaging. The accuracy of the velocity reconstruction is quantified by reporting the mean, the standard deviation and the uncertainty of the mean of streamwise velocity outside the separated flow region at x/D = 0.5, y/D = 0.8 and z/D = 0; These are respectively $\mu = 1.13$, $\sigma = 0.09$ and $U_\mu = 0.02$ relative to the freestream velocity. Finally, it is observed that the wake center slightly moves downward at increasing distances behind the sphere (Fig. 6-left), which is ascribed to the interference with the supporting rod.

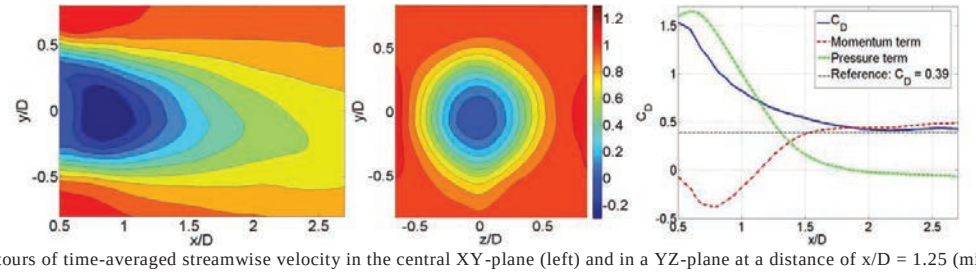

Fig. 6. Contours of time-averaged streamwise velocity in the central XY-plane (left) and in a YZ-plane at a distance of x/D = 1.25 (middle). At the right the computed drag coefficient, and the momentum and pressure terms, at increasing distances behind the sphere (reference value of 0.39 [20]).

Fig. 6-right presents the drag coefficient computed from velocity and pressure fields in the wake of the model. The figure also shows the separate momentum and pressure terms that contribute to the drag coefficient, as well as a reference value reported by Constantinescu and Squires [21]. It is observed that the drag coefficient reaches a relative steady value of about 0.45 after x/D = 1.7. Constantinescu and Squires report a drag coefficient of 0.39 and Achenbach [10] a value of 0.4. Considering the individual momentum and pressure terms, it is observed that the pressure term is high at small x/D, after which it slowly decreases. After about x/D = 1.7 it fluctuates around zero. The momentum term is negative at small x/D, after which it increases to a steady value of about 0.45. It can be concluded that the drag coefficient can be estimated solely from the momentum term if the velocity field is taken sufficiently far from the object [14]. In this case, two sphere diameters downstream seems to be sufficient. The drag coefficient calculated at x/d = 2 over all twenty data sets is 0.42. C_D calculated over the first ten is 0.45 and over the last ten 0.38. Hence, the uncertainty of the calculated drag coefficients is estimated to be about 7%.

Below x/D = 1.7 the approach clearly overestimates the drag. This can be partly explained by an overestimation of the pressure in the near wake. The computed base pressure is about -0.5, while a value around -0.3 is expected [10, 22]. Also inaccuracies of the momentum term contribute to the overestimation of the drag. In the near wake, the velocity in the measurement domain does not recover to the freestream conditions, but to a value higher than the freestream value (Fig. 6-left, for example x/D = 0.5, y/D = ±0.8), resulting in an underestimation of the momentum term too. Other inaccuracies in the computation of the drag coefficient result from the presence of the rod that supports the sphere and blockage (about 8%), contributing to overestimate the drag coefficient.

Despite the limitations, the proposed approach appears to be suitable for the estimate the drag coefficient of a moving object. The comparison with literature sets the current approach to within 15% accuracy.

5. Conclusions

A methodology is discussed to compute drag from velocity data measured in the wake of a stationary or moving model. The methodology is applicable to speed sports and is demonstrated in two different applications.
Planar PIV measurements are conducted in the wake of a cylinder dressed in two different fabrics, one smooth and one rough. The whole-field data obtained from the PIV measurement clearly show the differences in the flow field between the two configurations, which are also observed in the computed drag. The application of the surface roughness reduces the drag coefficient by 32%, from 1.1 to 0.75.

A small-scale system is developed that performs tomographic PIV measurements on a 16 cm sphere transiting across the measurement domain. The drag coefficient of the sphere is computed within 15% accuracy with respect to literature. Applications of the discussed techniques are envisaged for speed sport aerodynamics.

References

[1] Sætran L and Oggiano L, Skin suit aerodynamics in speed skating, in Sport Aerodynamics, Helge Nørstrud Editor, 2008.
[2] Gibertini Gand Grassi D. Cycling Aerodynamics. in Sport Aerodynamics. Helge Nørstrud Editor. 2008.
[3] Lukes RA, Chin SB, Haake SJ. The understanding and development of cycling aerodynamics. Sports Engineering 8, 2005; 59-74.
[4] Crouch TN, Burton D, Brown NAT, Thomson MC, Sheridan J. Flow topology in the wake of a cyclist and its effect on aerodynamic drag. J. Fluid Mech. 2014; Vol. 748. P. 5-35.
[5] Grappe F, Candau R, Belli A, Rouillon JD. Aerodynamic drag in field cycling with special reference to Obree's position, Ergonomics, 1997; vol. 40. no. 12. pp. 1299 – 1311.
[6] Pugh LGCE. The relation of oxygen intake and speed in competition cycling and comparative observations on the bicycle ergometer. J. Physiol. 1974; 241 p. 795-808.
[7] van Oudheusden BW. PIV-based pressure measurement. Meas. Sci. Technol.; 2013. Vol 24. 32 p.
[8] Raffel M, Willert C E, Wereley S T and Kompenhans. Particle Image Velocimetry. A Practical Guide;2007. 2nd edn (Berlin:Springer)
[9] Chabroux V, Mba MN, Sainton P, Favier D. Wake characteristics of time trial helmets using PIV-3C technique. 15th Int. Symp. on Appl. of Laser Tech. to Fl. Mech. Lisbon; 2010.
[10] Achenbach E. Experiments on the flow past spheres at very high Reynolds numbers. J. Fluid Mech.; 1972. vol. 54. part 3. pp. 565-575
[11] Achenbach E and Heinecke E. On vortex shedding from smooth and rough cylinders in the range of Reynolds numbers $6x10^3$ to $5x10^6$. J. Fluid Mech.; 1981. vol. 109. pp. 239-251.
[12] Oggiano L, Browlie L, Troynikov O, Bardal LM, Seater C, Seatran L. A review on skin suits and sport garment aerodynamics: guidelines and state of the art. Procedia Engineering 60. APCST; 2013. pp. 91-98.
[13] Zdravkovich MM, Aerodynamic of bicycle wheel and frame, J. of Wind Engineering and Industrial Aerodynamics; 1990. vol. 40, pp. 55-70.
[14] Anderson Jr JD, Fundamentals of aerodynamics, McGraw-Hill International editions; 1991.
[15] Ragni D, van Oudheusden BW, Scarano F. Non-intrusive aerodynamic load analysis of an aircraft propeller blade. Exp Fl.; 2011. 51:361-371.
[16] Oggiano L, Troynikov O, Konopov I, Subic A, Alam F. Aerodynamic bahaviour of single sport jersey fabrics with different roughness and cover factors. Sport Eng.; 2009. 12:1:12.
[17] Fage A, Warsap GH. The effect of turbulence and surface roughness on the drag of a circular cylinder. British Aerospace Resourse Council, memo 1283; 1929.
[18] Lynch KP and Scarano F. An efficient and accurate approach to MTE-MART for time-resolved tomographic PIV, Exp. Fluids; 2015. pp 56:66.
[19] Jang YI and Lee SJ. PIV analysis of near-wake behind a sphere at a subcritical conditions. Exp Fluids; 2008. 44:905–914.
[20] Ozgoren M, Okbaz A, Kahraman A, Hassanzadeh R, Sahin B, Akilli H, Dogan S. Experimental Investigation of the Flow structure around a sphere and its control with jet flow via PIV, 6th Int. Adv. Techn. Symposium, Elazığ, Turkey; 2011.
[21] Constantinescu GS and Squires KD. LES and DES Investigations of Turbulent Flow over a Sphere at Re=10000. Flow, Turbulence and Combustion; 2003. 70: 267–298.
[22] Bakic V, Schmid M, Stankovic Bf. Experimental investigation of turbulent structures of flow around a sphere. Thermal Science; 2006. vol. 10, no. 2. pp. 97-112.